Green rust formation controls nutrient availability in a ferruginous water column

Asfaw Zegeye[1,2], Steeve Bonneville[3,4], Liane G. Benning[3], Arne Sturm[5], David A. Fowle[5], CarriAyne Jones[6], Donald E. Canfield[6], Christian Ruby[2], Lachlan C. MacLean[7], Sulung Nomosatryo[8], Sean A. Crowe[6], and Simon W. Poulton[1]

[1]School of Civil Engineering and Geosciences, Newcastle University, Drummond Building, Newcastle upon Tyne NE1 7RU, UK

[2]Laboratoire de Chimie Physique et Microbiologie pour l'Environnement (LCPME), UMR 7564 CNRS, Université Henri Poincaré-Nancy 1, France

[3]School of Earth and Environment, University of Leeds, Leeds LS2 9JT, UK

[4]Departement des Sciences de la Terre et l'Environnement, Université Libre de Bruxelles, 50 Av. F.D. Roosevelt, 1050 Bruxelles, Belgium

[5]Department of Geology, University of Kansas, Lawrence, Kansas 66047, USA

[6]Nordic Center for Earth Evolution (NordCEE) and Institute of Biology, University of Southern Denmark, Campusvej 55, 5230 Odense M, Denmark

[7]Canadian Light Source, 101 Perimeter Road, Saskatoon S7N 0X4, Canada

[8]Research Center for Limnology, Indonesian Institute of Sciences (LIPI), Cibinong-Bogor, Indonesia

ABSTRACT

Iron-rich (ferruginous) conditions were a prevalent feature of the ocean throughout much of Earth's history. The nature of elemental cycling in such settings is poorly understood, however, thus hampering reconstruction of paleoenvironmental conditions during key periods in Earth evolution. This is particularly true regarding controls on nutrient bioavailability, which is intimately linked to Earth's oxygenation history. Elemental scavenging during precipitation of iron minerals exerts a major control on nutrient cycling in ferruginous basins, and the predictable nature of removal processes provides a mechanism for reconstructing ancient ocean chemistry. Such reconstructions depend, however, on precise knowledge of the iron minerals formed in the water column. Here, we combine mineralogical and geochemical analyses to demonstrate formation of the mixed-valence iron mineral, green rust, in ferruginous Lake Matano, Indonesia. Carbonated green rust (GR1), along with significant amounts of magnetite, forms below the chemocline via the reduction of ferrihydrite. Further, we show that uptake of dissolved nickel, a key micronutrient required for methanogenesis, is significantly enhanced during green rust formation, suggesting a major control on methane production in ancient ferruginous settings.

INTRODUCTION

The chemistry of the ocean has varied greatly through Earth's history. In contrast to the dominantly well-oxygenated condition of the modern ocean, anoxic deep ocean conditions likely prevailed throughout much of the Precambrian (Holland, 1984; Canfield et al., 2008) and at various times in the Phanerozoic (Jenkyns, 2010). During most of the Precambrian, anoxic deep ocean waters were likely ferruginous, as indicated both by the extensive deposition of banded iron formations up until ca. 1.8 b.y. ago, and by the chemical nature of Fe enrichments in marine sediments deposited throughout much of the subsequent Proterozoic (Canfield et al., 2008; Poulton et al., 2010; Planavsky et al., 2011). For Phanerozoic oceanic anoxic events (OAEs), widespread euxinic conditions are commonly envisaged (Jenkyns, 2010). However, emerging insight suggests that redox conditions may have fluctuated between euxinic and ferruginous during Phanerozoic OAEs, leading to fundamental differences in nutrient cycling (März et al., 2008).

Freshly precipitated Fe minerals such as ferrihydrite are believed to exert a strong influence on nutrient availability under ferruginous conditions, and thus ferrihydrite has been the model mineral for reconstructing P and Ni bioavailability in the ancient ocean (Konhauser et al., 2009; Planavsky et al., 2010). However, while ferrihydrite commonly precipitates during dissolved Fe^{2+} oxidation under oxic oceanic conditions, other Fe minerals could form during anaerobic oxidation pathways (e.g., Kappler and Newman, 2004). Here, we investigate the geochemistry and mineralogy of Fe in ferruginous Lake Matano, Indonesia. Within the chemocline, Fe^{2+} is oxidized, generating authigenic mineral particles (Crowe et al., 2008a). Lake Matano thus represents an ideal location to explore mineralization processes and nutrient cycling under ferruginous conditions.

METHODS

Full details of sampling protocols and methods are provided in the GSA Data Repository[1]. Water column particulates were collected by filtering water pumped from depth through an in-line filtration device under N_2. Filters were transferred to airtight vials and stored in the dark at 4 °C until analysis. Particulate Fe speciation was determined via a modified sequential extraction procedure (Poulton and Canfield, 2005). This technique operationally defines the proportion of Fe that is considered highly reactive (Fe_{HR}) toward reductive dissolution, consisting of hydrous ferric oxides (e.g., ferrihydrite: $Fe(III)_{HFO}$), reduced particulate Fe (e.g., adsorbed Fe^{2+}, $FeCO_3$: $Fe(II)_{red}$), crystalline ferric (oxyhydr)oxides (e.g., goethite: Fe_{ox}), and magnetite (Fe_{mag}).

Scanning electron microscopy (SEM) and energy-dispersive spectrometry (EDS) were conducted on filters that were stub-mounted and gold-sputter-coated. For transmission electron microscopy (TEM), particles were deposited onto a carbon Cu TEM grid and dried at room temperature under anoxic conditions. Samples were transported in an anoxic transfer chamber and loaded onto the TEM (within a few seconds of opening the transfer chamber). For synchrotron X-ray spectroscopic analyses (μX-ray fluorescence [μXRF] and μX-ray diffraction [μXRD]), particles were mounted on Kapton™ film and sealed in Kapton™ tape under N_2.

WATER COLUMN CHEMISTRY

Water column profiles are presented in Figure 1. Oxygen was undetectable (<1 μmol L^{-1}) below 120.1 m, and dissolved Fe^{2+} was first detected at 120.5 m, reaching stable concentrations of ~60 μmol L^{-1} at 135 m over the three sampling days. Ferrihydrite ($Fe(III)_{HFO}$) is formed from the oxidation of Fe^{2+} at the oxycline, and this accounts for the presence of $Fe(III)_{HFO}$ above the depth where Fe^{2+} first accumulates (Fig. 1B). This Fe(III) pool is reduced below the oxycline, resulting in an increase in $Fe(II)_{red}$ with depth and complete reduction of the $Fe(III)_{HFO}$ pool in the

[1]GSA Data Repository item 2012180, expanded sampling details and methods, is available online at www.geosociety.org/pubs/ft2012.htm, or on request from editing@geosociety.org or Documents Secretary, GSA, P.O. Box 9140, Boulder, CO 80301, USA.

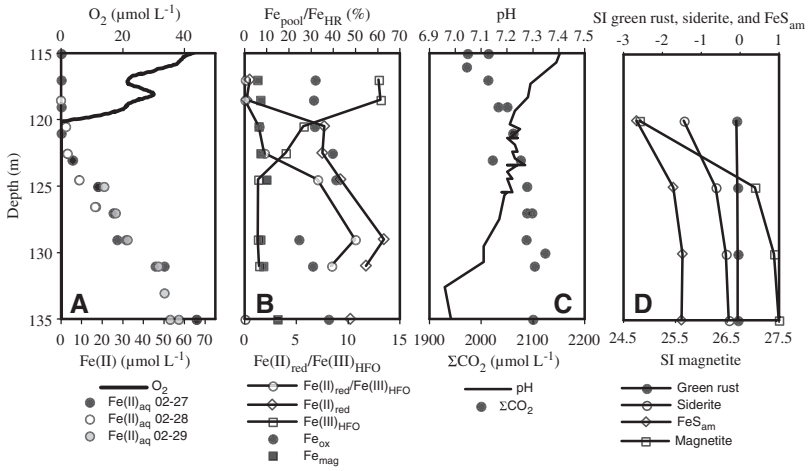

Figure 1. Water column geochemical and saturation index (SI) profiles. A: Dissolved O_2 and Fe(II). 02-27, 02-28, and 02-29 refer to sampling dates in 2009. B: Particulate Fe partitioning. Highly reactive Fe (Fe_{HR}) = $Fe(II)_{red}$ + $Fe(III)_{HFO}$ + Fe_{ox} + Fe_{mag}. Fe_{pool} refers to each Fe fraction. Data at 135 m refer to sediment 0–0.5 cm below the sediment-water interface (214 m water depth), and $Fe(II)_{red}$ includes Fe present as sulfides (~21% of Fe_{HR}). C: Total dissolved inorganic carbon (ΣCO_2) and pH values used to calculate SI profiles. D: SI profiles for carbonated green rust (GR1), siderite, FeS_{am} (amorphous FeS), and magnetite. Note separate scale for magnetite. Values above zero indicate saturation.

underlying sediments. The extractions also indicate significant concentrations of magnetite (Fe_{mag}), increasing to ~15% of Fe_{HR} content in deposited sediments, consistent with the saturated state of waters below 125 m with respect to magnetite (Fig. 1D). This observation is supported by magnetic studies of deposited sediments, which confirm the presence of high concentrations of nanoparticulate magnetite or titanomagnetite (Crowe et al., 2004). Crystalline ferric (oxyhydr)oxide minerals (dominantly goethite: Fe_{ox}) remain essentially constant with depth (Fe_{ox}/Fe_{HR} = 0.33 ± 0.06), demonstrating that ferrihydrite ($Fe(III)_{HFO}$) is the dominant precursor mineral from which the $Fe(II)_{red}$ and Fe_{mag} fractions ultimately form.

PARTICLE MINERALOGY

Examination of water column particulates by SEM reveals the presence of hexagonal plates of up to ~400 nm width in the upper chemocline at 118 m (Fig. 2A). Abundant nanoparticulate clusters are also observed at this depth (Fig. 2B), which, based on the chemical extraction data, likely represent ferrihydrite or nanogoethite (Fig. 2B). TEM analysis shows similar hexagonal plates at 131 m (Fig. 2C) and 132.5 m (Fig. 2D). Selected area electron diffraction patterns generated from particles at 132.5 m reveal several crystalline minerals with d_{hkl} (interplanar spacing) values (spots 1–7; Fig. 2E; Table 1) corresponding to the mixed

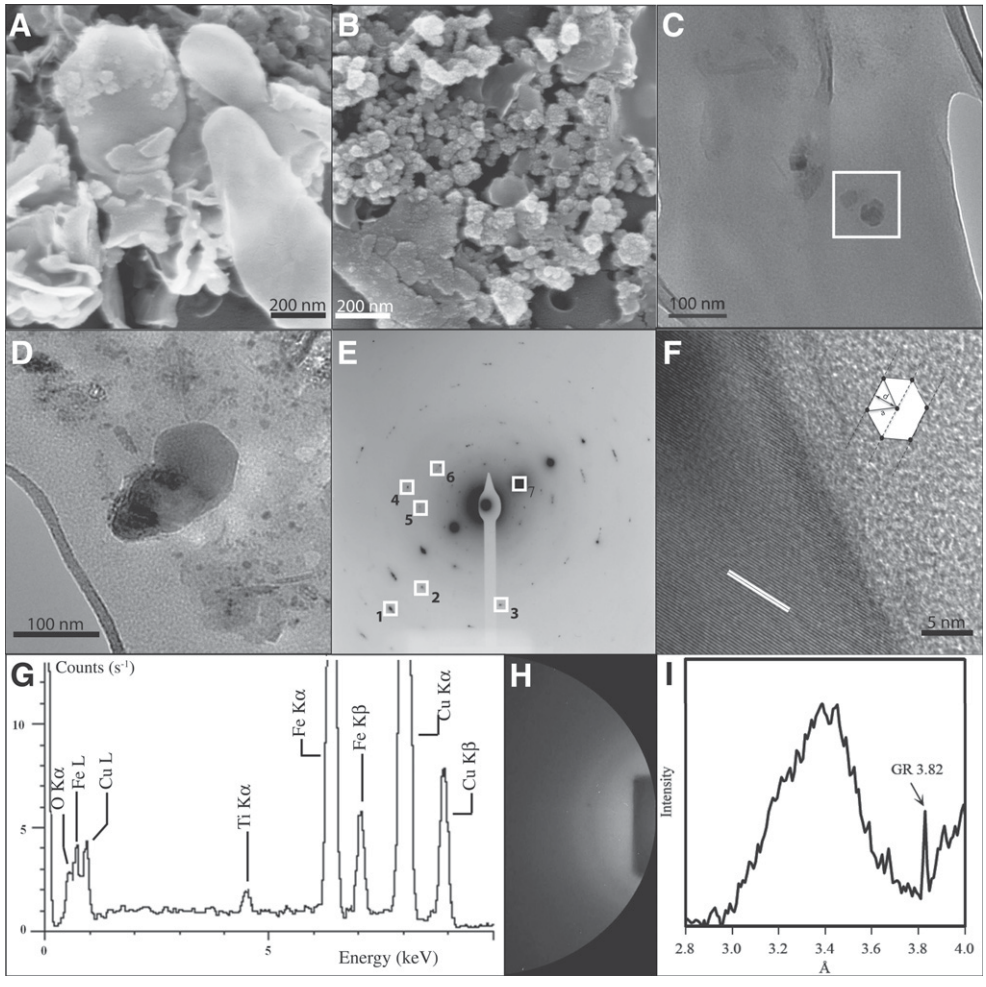

Figure 2. A: Scanning electron microscopy (SEM) image of hexagonal green rust (GR) from 118 m depth (upper limit of the chemocline). B: SEM image showing poorly crystalline mineral aggregates (probably ferrihydrite or nanoparticulate goethite) at 118 m depth. C: Transmission electron microscopy (TEM) image of hexagonal GR from 131 m depth. D: TEM image showing hexagonal GR and nanoparticulates (possibly magnetite) at 132.5 m depth. E: Selected area electron diffraction pattern of the GR mineral from D. Numbers correspond to representative spots of different diffraction rings used to calculate the d_{hkl} (interplanar spacing) parameters reported in Table 1. F: High-resolution TEM image of a GR particle at 132.5 m, including a schematic representation of the lattice fringes with a d-spacing of 2.793 Å characteristic of the (100) plane of a GR1 crystal. Dashed lines represent lattice fringes, while black dots correspond to Fe cations with a = 3.175 Å. G: Energy-dispersive spectrometry trace for the GR mineral at 132.5 m. The Cu signal arises from the sample grid. H: Two-dimensional μX-ray diffraction (μXRD) charge-coupled device (CCD) image of particles at 123.5 m depth. I: One-dimensional diffraction pattern for the image shown in H. The peak at 3.82 Å is characteristic of the (hkl 006) plane of GR1. The more intense (003) plane could not be observed due to the large beam stop blocking any diffraction spots at low angles. The broad peak at ~3.4 Å is from the Kapton™ sample cover.

TABLE 1. INTERPLANAR DISTANCES (d_{hkl})

	Sample d_{hkl} (Å)	GR d_{hkl} (Å)	Reference
SAED spot 1	2.610 ± 0.142	2.647	1
2	1.664 ± 0.057	1.631	1
3	1.457 ± 0.044	1.453	1
4	1.226 ± 0.031	1.216	2
5	1.035 ± 0.022	1.034–1.038	2
6	0.970 ± 0.019	0.975	2
7	0.728 ± 0.011	0.7265	2
HR-TEM	2.793 ± 0.050	2.75	1
μXRD	3.82	3.80	1

Note: Distances are extracted from selected area electron diffraction (SAED) analysis (Fig. 2E) of the hexagonal crystal shown in Figure 2D, from high-resolution transmission electron microscopy (HR-TEM) analysis shown in Figure 2F, and from synchrotron-based μX-ray diffraction (μXRD) shown in Figure 2I. d_{hkl} values are also included for synthetic GR. References: 1—Drissi et al., 1995; 2—Génin et al., 2006.

Fe(II)/Fe(III) hydroxide, carbonated green rust (GR1). This is confirmed by the hexagonal morphology of the crystals (Ahmed et al., 2010) and the high-resolution TEM image of the crystal viewed parallel to the (001) plane, which shows a lattice spacing of 2.793 ± 0.05 Å (Fig. 2F), characteristic of the (100) plane of GR1. The elemental composition of the same particle determined by EDS (Fig. 2G) is also consistent with GR1. Further evidence comes from the synchrotron-based XRD pattern generated from particles at 123.5 m water depth. The Debye ring observed on the image in Figure 2H translates to a d-spacing of 3.82 Å (Fig. 2I), which corresponds to the (006) lattice plane of GR1 (Génin et al., 2006).

We provide the first identification of green rust (also referred to as "fougerite" in nature) in a stratified water body. Green rust has a general formula of $[Fe^{II}_{(1-x)}Fe^{III}_{x}(OH)_2]^{x+} \cdot [(x/n)A^{n-} \cdot (m/n)H_2O]^{x-}$. It is a layered double hydroxide consisting of positively charged brucite-type tri-octahedral sheets separated by an interlayer containing various anions (A^{n-} = CO_3^{2-}, SO_4^{2-}, Cl^-, OH^-) and m water molecules (Génin et al., 1996). The water below 120 m depth is saturated with respect to GR1 (Fig. 1D), so its formation is thermodynamically favorable. However, the Fe(II)/Fe(III) ratio in GR1 is commonly 2–3 (Hansen, 2001), which is lower than the ratio observed below the chemocline in Lake Matano (Fig. 1B). Therefore, a form of Fe(II) other than GR1 likely also contributes to the particulate $Fe(II)_{red}$ fraction at depth. Siderite and FeS are potential candidates, but water at these depths is undersaturated with respect to both of these phases (Fig. 1D). Thus they are unlikely to contribute to the $Fe(II)_{red}$ pool, although we cannot discount the possibility that metastable phases may form in minor quantities. Instead, the excess Fe(II) is likely present as Fe^{2+} adsorbed onto particle surfaces (Parmar et al., 2001).

Green rust forms during photoferrotrophy in bacterial cultures (Kappler and Newman, 2004). Photoferrotrophy appears to be a prevalent process at the chemocline in Lake Matano (Crowe et al., 2008a), but during our sampling in 2009, photoferrotrophs were nearly absent (as indicated by very low bacteriochlorophyll *e* concentrations), due to a deepening of the pycnocline below the depth of light penetration. A microbial origin for GR remains a possibility, though, because GR can form as a major product (together with more minor quantities of magnetite) during the reduction of ferric oxides via dissimilatory Fe reduction (Parmar et al., 2001; O'Loughlin et al., 2007; Zegeye et al., 2007). Green rust (and magnetite) can also form from the abiotic solid-phase transformation of ferrihydrite following Fe^{2+} adsorption (Sumoondur et al., 2008), and from the reaction of Fe^{2+} with Mn oxide (Postma, 1985), both of which could be important pathways in Lake Matano. Regardless of the precise formation pathway, our documentation of GR throughout the chemocline attests both to GR (meta)stability under ferruginous conditions and to its role in Fe-mineral redox transformations.

NUTRIENT UPTAKE

Green rust has a strong adsorptive capacity for anions (Randall et al., 2001) and trace metals (Parmar et al., 2001), implying that formation of GR would likely exert a major control on macro- and micronutrient cycling under ferruginous conditions. We explore this by considering the role of GR in Ni cycling in Lake Matano. Nickel is a key metal cofactor in hydrogenases and methyl-coenzyme M reductase, which is used by methanogens to generate methane. Reconstructions based on Ni uptake by ferrihydrite suggest stepwise decreases in oceanic Ni concentrations through time (Konhauser et al., 2009). This may have limited rates of methanogenesis, thus depleting a major atmospheric sink for O_2 and driving the oxygenation of Earth's atmosphere (Konhauser et al., 2009). However, the scavenging efficiency of Ni by GR is particularly high, and dissolved Ni^{2+} is largely immobilized in response to GR formation during bacterial reduction of ferrihydrite (Parmar et al., 2001). Abiotic GR formation also effectively scavenges Ni^{2+} from solution through both substitution into the mineral structure and adsorption (Chaves et al., 2007). Thus, reconstruction of Ni concentrations through time requires detailed understanding of the relative roles of ferrihydrite and GR in Ni uptake under ferruginous conditions.

Nickel uptake by the most reactive Fe fraction in our extractions (i.e., ferrihydrite and GR) increases significantly with depth below the chemocline (Fig. 3A), suggesting Ni uptake as ferrihydrite is transformed to GR. This observation is supported by synchrotron μXRF analyses. Particles at 118 m (Fig. 3B) show a strong linear relationship between Ni and Fe, which likely relates to Ni associated with ferrihydrite and goethite, the dominant Fe phases at this depth (goethite is introduced to the basin as a weathering product and is a major particulate source of Ni; Crowe et al., 2008b). At 129 m, Ni-Fe associations suggest two distinct particle populations (Fig. 3C). In the dominant population, Ni correlates strongly with Fe, but with a steeper slope than the particles at 118 m, demonstrating more effective Ni uptake, consistent with the chemical extraction results (Fig. 3A). Because most of the ferrihydrite has been reduced at this depth (Fig. 1) and because magnetite is not an effective scavenger of Ni (Parmar et al., 2001), this population likely represents Ni associated with GR and goethite. The more minor population shows highly variable Ni, but no relationship with Fe. We suggest that this represents water column formation of a non-Fe-associated Ni phase, which is likely to be Ni sulfide (Crowe et al., 2008b) or possibly Ni associated with organic matter, but this is negligible relative to the Fe-associated phase.

Since the μXRF analyses include Ni associated with goethite, we use the Ni and Fe extraction data to examine the relative efficiency of dissolved Ni uptake as ferrihydrite is converted to GR, via comparison of the distribution coefficients (K_D) obtained at 118 m and 129 m (this

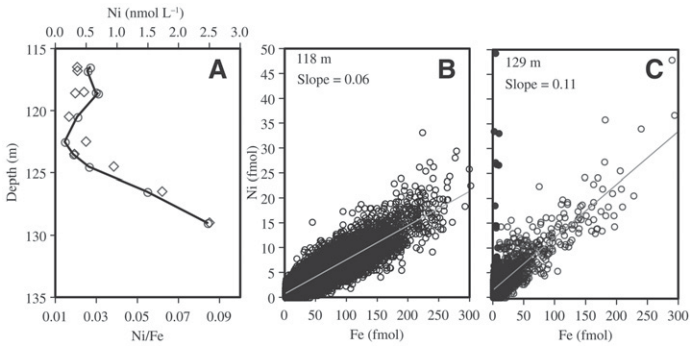

Figure 3. A: Particulate Ni concentration (open circles) in the most reactive Fe fraction (comprising $Fe(II)_{red}$ plus $Fe(III)_{HFO}$) and the ratio relative to $Fe(II)_{red}$ plus $Fe(III)_{HFO}$ (open diamonds). B: Synchrotron μXRF of particles at 118 m depth. C: Synchrotron μXRF of particles at 129 m depth. Filled circles represent particles attributed to NiS or organic matter; open circles represent Ni attributed to Fe minerals.

comparison is valid because particulate Fe concentrations are similar at these two depths):

$$\left(\frac{\mathrm{Ni_{part}}}{\mathrm{Fe_{part}}}\right) = K_{\mathrm{D}}\left[\mathrm{Ni_{aq}}\right]. \quad (1)$$

Nickel concentrations are 31 nM at 118 m and 50 nM at 129 m, suggesting that the GR-rich particles at 129 m are approximately three times more efficient at scavenging Ni than the ferrihydrite-rich particles at 118 m (see the Data Repository). It should be noted that a corresponding threefold decrease in dissolved Ni does not occur over this interval, because Ni is largely sourced from reductive dissolution of goethite at depth and the water column is not well mixed above and below the chemocline. However, this does not affect the validity of our Ni uptake comparison of the two minerals based on the calculated distribution coefficients.

IMPLICATIONS

The elemental control that GR exerts in ferruginous settings clearly has important implications for reconstructions of both macro- and micronutrients in the ancient oceans. Unlike the early Precambrian, however, dissolved silica in Lake Matano (300–420 μ*M*; Crowe et al., 2008a) is below saturation with respect to cristobalite (0.67 mM) and amorphous silica (2.20 mM). Although the impact of higher silica concentrations on the uptake of Ni by GR is not known, silica has been shown to have a significant influence on Ni uptake by ferrihydrite (Konhauser et al., 2009), and thus our results are not currently directly applicable to reconstructions of dissolved Ni in the early Precambrian (although they are more comparable to later time periods). Our findings do, however, indicate that paleoreconstructions of dissolved nutrient concentrations based on the adsorption characteristics of ferrihydrite require re-evaluation.

Green rust is also an important precursor during magnetite formation (Sumoondur et al., 2008). Our observation that magnetite begins to form in the water column, probably via transformation from GR, suggests that some of the magnetite found in sediments deposited under ferruginous conditions is likely syngenetic in origin. Overall, we assert that GR is likely much more prevalent in the environment than has previously been recognized, and we suggest that the role of GR in a variety of elemental cycles is significant, and thus requires careful consideration, in studies of both modern and ancient ferruginous environments.

ACKNOWLEDGMENTS

Work was funded by Danmarks Grundforskningsfond, the Natural Sciences and Engineering Research Council of Canada, the Agouron Institute, the Natural Environment Research Council, and the U.S. National Science Foundation. PT International Nickel Indonesia Tbk, P. Sampetoding, D. Rahim, S. Bungin, L. Lubis-Nuria, and S. Rio provided logistical support. Kurt Konhauser and two anonymous reviewers are thanked for helpful suggestions.

REFERENCES CITED

Ahmed, I.A.M., Benning, L.G., Kakonyi, G., Sumoondur, A., Terril, N., and Shaw, S., 2010, Formation of green rust sulfate: A combined in situ time-resolved X-ray scattering and electrochemical study: Langmuir, v. 26, p. 6593–6603, doi:10.1021/la903935j.

Canfield, D.E., Poulton, S.W., Knoll, A.H., Narbonne, G.M., Ross, G., Goldberg, T., and Strauss, H., 2008, Ferruginous conditions dominated later Neoproterozoic deep-water chemistry: Science, v. 321, p. 949–952, doi:10.1126/science.1154499.

Chaves, L.H.G., Curry, J.E., Stone, D.A., and Chorover, J., 2007, Fate of nickel ion in (II-III) hydroxysulphate green rust synthesized by precipitation and coprecipitation: Revista Brasileira de Ciencia do Solo, v. 31, p. 813–818, doi:10.1590/S0100-06832007000400021.

Crowe, S.A., Pannalal, S.J., Fowle, D.A., Cioppa, M.T., Symons, D.T.A., Haffner, G.D., Fryer, B.J., McNeely, R., Sundby, B., and Hehanussa, P.E., 2004, Biogeochemical cycling in Fe-rich sediments from Lake Matano, Indonesia: 13th International Symposium on Water-Rock Interaction, p. 1185–1189.

Crowe, S.A., Jones, C., Katsev, S., Magen, C., O'Neill, A.H., Sturm, A., Canfield, D.E., Haffner, G.D., Mucci, A., Sundby, B., and Fowle, D.A., 2008a, Photoferrotrophs thrive in an Archean ocean analogue: Proceedings of the National Academy of Sciences of the United States of America, v. 105, p. 15,938–15,943, doi:10.1073/pnas.0805313105.

Crowe, S.A., O'Neill, A.H., Katsev, S., Hehanussa, P., Haffner, G.D., Sundby, B., Mucci, A., and Fowle, D.A., 2008b, The biogeochemistry of tropical lakes: A case study from Lake Matano, Indonesia: Limnology and Oceanography, v. 53, p. 319–331, doi:10.4319/lo.2008.53.1.0319.

Drissi, S.H., Refait, Ph., Abdelmoula, M., and Génin, J.M.R., 1995, The preparation and thermodynamic properties of Fe(II)-Fe(III) hydroxide-carbonate (green rust 1); Pourbaix diagram of iron in carbonate-containing aqueous media: Corrosion Science, v. 37, p. 2025–2041, doi:10.1016/0010-938X(95)00096-3.

Génin, J.-M.R., Olowe, A.A., Refait, P., and Simon, L., 1996, On the stoichiometry and Pourbaix diagram of Fe(II)-Fe(III) hydroxy-sulphate or sulphate-containing green rust 2: An electrochemical and Mössbauer spectroscopic study: Corrosion Science, v. 38, p. 1751–1762, doi:10.1016/S0010-938X(96)00072-8.

Génin, J.-M.R., Ruby, C., Gehin, A., and Refait, P., 2006, Synthesis of green rusts by oxidation of $Fe(OH)_2$, their products of oxidation and reduction of ferric oxyhydroxides; *E*h-pH Pourbaix diagrams: Comptes Rendus Geoscience, v. 338, p. 433–446, doi:10.1016/j.crte.2006.04.004.

Hansen, H.C.B., 2001, Environmental chemistry of iron(II)-iron(III) LDHs (green rusts), *in* Rives, V., ed., Layered double hydroxides: Present and future: New York, Nova Science Publishers, p. 469–493.

Holland, H.D., 1984, Chemical evolution of the atmosphere and oceans: Princeton, New Jersey, Princeton University Press, 598 p.

Jenkyns, H.C., 2010, Geochemistry of oceanic anoxic events: Geochemistry, Geophysics, Geosystems, v. 11, Q03004, doi:10.1029/2009GC002788.

Kappler, A., and Newman, D.K., 2004, Formation of Fe(III)-minerals by Fe(II)-oxidizing photoautotrophic bacteria: Geochimica et Cosmochimica Acta, v. 68, p. 1217–1226, doi:10.1016/j.gca.2003.09.006.

Konhauser, K.O., Pecoits, E., Lalonde, S.V., Papineau, D., Nisbet, E.G., Barley, M.E., Arndt, N.T., Zahnle, K., and Kamber, B.S., 2009, Ocean nickel depletion and a methanogen famine before the Great Oxidation Event: Nature, v. 458, p. 750–753, doi:10.1038/nature07858.

März, C., Poulton, S.W., Beckmann, B., Küster, K., Wagner, T., and Kasten, S., 2008, Redox sensitivity of P cycling during marine black shale formation: Dynamics of sulfidic and anoxic, non-sulfidic bottom waters: Geochimica et Cosmochimica Acta, v. 72, p. 3703–3717, doi:10.1016/j.gca.2008.04.025.

O'Loughlin, E.J., Larese-Casanova, P., Scherer, M., and Cook, R., 2007, Green rust formation from the bioreduction of γ-FeOOH (lepidocrocite): Comparison of several *Shewanella* species: Geomicrobiology Journal, v. 24, p. 211–230, doi:10.1080/01490450701459333.

Parmar, N., Gorby, Y.A., Beveridge, T.J., and Ferris, F.G., 2001, Formation of green rust and immobilization of nickel in response to bacterial reduction of hydrous ferric oxide: Geomicrobiology Journal, v. 18, p. 375–385, doi:10.1080/014904501753210549.

Planavsky, N.J., Rouxel, O.J., Bekker, A., Lalonde, S.V., Konhauser, K.O., Reinhard, C.T., and Lyons, T.W., 2010, The evolution of the marine phosphate reservoir: Nature, v. 467, p. 1088–1090, doi:10.1038/nature09485.

Planavsky, N.J., McGoldrick, P., Scott, C.T., Li, C., Reinhard, C.T., Kelly, A.E., Chu, X., Bekker, A., Love, G.D., and Lyons, T.W., 2011, Widespread iron-rich conditions in the mid-Proterozoic ocean: Nature, v. 477, p. 448–451, doi:10.1038/nature10327.

Postma, D., 1985, Concentration of Mn and separation from Fe in sediments—I. Kinetics and stoichiometry of the reaction between birnessite and dissolved Fe(II) at 10°C: Geochimica et Cosmochimica Acta, v. 49, p. 1023–1033, doi:10.1016/0016-7037(85)90316-3.

Poulton, S.W., and Canfield, D.E., 2005, Development of a sequential extraction procedure for iron: Implications for iron partitioning in continentally derived particulates: Chemical Geology, v. 214, p. 209–221, doi:10.1016/j.chemgeo.2004.09.003.

Poulton, S.W., Fralick, P.W., and Canfield, D.E., 2010, Spatial variability in oceanic redox structure 1.8 billion years ago: Nature Geoscience, v. 3, p. 486–490, doi:10.1038/ngeo889.

Randall, S.R., Sherman, D.M., and Ragnarsdottir, K.V., 2001, Sorption of As(V) on green rust ($Fe_4(II)Fe_2(III)(OH)_{12}SO_4 \cdot 3H_2O$) and lepidocrocite (γ-FeOOH): Surface complexes from EXAFS spectroscopy: Geochimica et Cosmochimica Acta, v. 65, p. 1015–1023, doi:10.1016/S0016-7037(00)00593-7.

Sumoondur, A., Shaw, S., Ahmed, I., and Benning, L.G., 2008, Green rust as a precursor for magnetite: An in situ synchrotron based study: Mineralogical Magazine, v. 72, p. 201–204, doi:10.1180/minmag.2008.072.1.201.

Zegeye, A., Ruby, C., and Jorand, F., 2007, Kinetic and thermodynamic analysis during dissimilatory γ-FeOOH reduction: Formation of green rust 1 and magnetite: Geomicrobiology Journal, v. 24, p. 51–64, doi:10.1080/01490450601134325.

Manuscript received 25 October 2011
Revised manuscript received 26 January 2012
Manuscript accepted 2 February 2012

Printed in USA